

**TIGHT COSMOLOGICAL CONSTRAINTS  
FROM THE ANGULAR-SIZE/REDSHIFT RELATION  
FOR ULTRA-COMPACT RADIO SOURCES**

by

J.C. Jackson<sup>1</sup>

School of Informatics

Division of Mathematics and Statistics

University of Northumbria at Newcastle

Ellison Building

Newcastle upon Tyne NE1 8ST, UK

**ABSTRACT**

Some years ago (Jackson and Dogson 1997) analysis of the angular-size/redshift relationship for ultra-compact radio sources indicated that for spatially flat universes the best choice of cosmological parameters was  $\Omega_m = 0.2$  and  $\Omega_\Lambda = 0.8$ . Here I present a new analysis of the original data set (Gurvits 1994), taking into account possible selection effects which bias against large objects; for flat universes figures are now  $\Omega_m = 0.24 + 0.09/-0.07$ . The data points match the corresponding theoretical curve very accurately out to  $z \sim 3$ , and there is clear and sustained indication of the switch from acceleration to deceleration, which occurs at  $z = 0.85$ .

**Key words:** cosmology – observations – theory – dark matter.

---

<sup>1</sup>e-mail: john.jackson@unn.ac.uk

## 1 INTRODUCTION

The default cosmological paradigm now is that we are living in a spatially flat accelerating Universe with matter (baryons plus Cold Dark Matter) and vacuum density-parameters  $\Omega_m = 0.27$  and  $\Omega_\Lambda = 0.73$  respectively, known as the concordance model. Definitive confirmation of a consensus which has been growing over the last two decades came with the recent Wilkinson Microwave Anisotropy Probe (WMAP) results (Spergel et al. 2003). The original evidence for such models was circumstantial, in that they reconcile the inflationary prediction of flatness with the observed low density of matter (Peebles 1984; Turner, Steigman & Kraus 1984). The first real evidence came from observations of very large-scale cosmological structures (Efstathiou, Sutherland & Maddox 1990), which paper clearly advocated everything that has come to be accepted in recent times: “.....very large scale cosmological structures can be accommodated in a spatially flat cosmology in which as much as 80 percent of the critical density is provided by a positive cosmological constant. In such a universe expansion was dominated by CDM until a recent epoch, but is now governed by the cosmological constant.” A similar case for this model was made by Ostriker and Steinhardt (1995), who also noted that the location and magnitude of the first Doppler peak in the cosmic microwave background (CMB) angular spectrum was marginally supportive of flatness. However, I think it is fair to say that the paradigm did not really begin to shift until the Hubble diagram for Type Ia supernovae (SNe Ia) (Schmidt et al. 1998; Riess et al. 1998; Perlmutter et al. 1999) provided reasonably convincing evidence that  $\Omega_\Lambda > 0$ ; the corresponding confidence region in the  $\Omega_m$ - $\Omega_\Lambda$  plane was large and elongated, but almost entirely confined to the positive quadrant. The dramatic impact of these results was probably occasioned by the simple nature of this classical cosmological test; coupled with accurate measures of the first Doppler peak in the CMB angular spectrum (Balbi et al. 2000; de Bernardis et al. 2000; Hanany et al. 2000), which established flatness to a high degree of accuracy, the SNe Ia results made anything but the concordance model virtually untenable. This paper is in part retrospective, and is about another simple classical cosmological test. Some years ago we published an analysis of the angular-size/redshift diagram for milliarcsecond radio-sources (Jackson & Dodson 1997; see also Jackson & Dodgson 1996), with a clear statement to the effect that “if the Universe is spatially flat, then models with low density are favoured; the best such model is  $\Omega_m = 0.2$  and  $\Omega_\Lambda = 0.8$ ” (to two significant figures the numbers would have been  $\Omega_m = 0.24$  and  $\Omega_\Lambda = 0.76$ ). These results pre-date the SNe Ia ones.

Ultra-compact radio sources were first used in this context by Kellermann (1993), who presented angular sizes for 79 objects, obtained using very-long-baseline interferometry (VLBI). These were divided into 7 bins according to redshift ( $z$ ), and the mean angular size ( $\theta$ ) plotted against the mean redshift for each bin. The main effect of Kellermann’s work was to establish that the resulting  $\theta$ - $z$  relationship was compatible with standard Friedmann-Lemaître-Robertson-Walker (FLRW) cosmological models, in sharp contrast to the case for the extended radio structures associated with radio-galaxies and quasars. In the latter case typical component separations are 30 arcseconds, and the observed relationship is the so-called Euclidean curve  $\theta \propto 1/z$  (Legg 1970; Miley 1971; Kellermann 1972; Wardle & Miley 1974); this deficit of large objects at high redshifts is believed to be an evolutionary effect, brought about by interaction with an evolving extra-galactic medium (Miley 1971; Barthel & Miley 1988; Singal 1988), or a selection effect, due to an inverse correlation between linear size and radio power (Jackson 1973; Richter 1973; Masson 1980; Nilsson et al. 1993). Ultra-compact objects have short lifetimes and are much smaller than their parent active galactic nuclei (AGNs), so that their local environment should be free of cosmological evolutionary effects, at least over an appropriate redshift range. However, it is not clear that observations of these objects are completely free from selection effects.

Kellermann’s work was extended by Gurvits (1994), who presented a large VLBI compilation,

based upon a 2.3 Ghz survey undertaken by Preston. et al. (1985), comprising 917 sources with a correlated flux limit of approximately 0.1 Jy; the sub-sample selected by Gurvits comprises 337 sources with known redshifts, and objective measures of angular size based upon fringe visibility (Thompson, Moran & Swenson 1986, p. 13). Gurvits gave good reasons for ignoring sources with  $z < 0.5$ , and using just the high-redshift data found marginal support for a low-density FLRW model, but considered only models with  $\Omega_\Lambda = 0$ . Jackson and Dogson (1997) was based upon Gurvits' sample, and considered 256 sources in the redshift range 0.511 to 3.787, divided into 16 bins of 16 objects. More recently Gurvits, Kellermann & Frey (1999) have presented a new compilation of 330 compact radio sources, observed at a somewhat higher frequency ( $\nu = 5$  GHz), which has stimulated a number of analyses (Cunha, Alcaniz & Lima 2002; Lima & Alcaniz 2002; Chen & Batra 2003; Jain, Dev & Alcaniz 2003), which consider the full  $\Omega_m$ - $\Omega_\Lambda$  plane. I think it is fair to say that the constraints placed upon cosmological parameters by this later work are significantly weaker than for example the SNe Ia constraints alone, and very much weaker than those obtained when the latter are coupled with CMB and Large Scale Structure observations (Efstathiou et al. 1999; Bridle et al. 1999; Lasenby, Bridle & Hobson 2000; Efstathiou et al. 2002).

The main purpose of this work is to show that when treated properly angular-size/redshift data place significant constraints upon cosmological parameters, comparable with those due to any of the currently fashionable tests taken in isolation. I find that the original Gurvits (1994) compilation better in this respect than the later compilation due to Gurvits et al. (1999), and I shall eventually discuss why this might be. Selection effects are discussed in Section 2, where evidence of such effects is found. Appropriate countermeasures are discussed in Section 3, and the corresponding results are presented as marginalised confidence regions in the  $\Omega_m$ - $\Omega_\Lambda$  plane, with some consideration of the quintessence parameter  $w$ . It is in the careful consideration of selection effects that this work is new, and differs from the analysis of essentially the same data in Jackson & Dodgson (1997), where such effects were ignored.

## 2 SELECTION EFFECTS

In a flux-limited sample sources observed at large redshifts are intrinsically the most powerful, so that an inverse correlation between size and radio luminosity will introduce a bias towards smaller objects. There are several reasons for expecting such a correlation. On quite general grounds we would expect sources to be expanding, and their luminosities to decrease with time after an initial rapid increase (Jackson 1973; Baldwin 1982; Blundell & Rawlings 1999). Additionally, relativistic beaming is important in compact sources, so that the apparent radio power increases and the angular size decreases when the beam is close to the line of sight. For this reason the use of compact sources as standard measuring rods has been questioned by Dabrowski, Lasenby and Saunders (1995). Dabrowski et al. (1995) use a simple model, comprising two identical but oppositely directed jets, and assume that the measured angular size corresponds to their separation projected onto the plane of the sky. This model might be very misleading, as the counter-jet would be very much fainter than the forward one, and the source would appear to be very asymmetric. Nevertheless, I have used their estimates of the effect of orientation bias upon estimates of cosmological parameters as a guide in what follows. The saving grace for cosmic radio sources is that their luminosities are known to increase rapidly with increasing  $z$  (Dunlop & Peacock 1990), which luminosity evolution allows sources of larger angular size to remain within the flux-limited sample; this effect is enhanced for compact sources, which typically have flat spectra, by the term  $(1+z)^{(1+\alpha)}$  in equation(2) below. For typical source parameters and a flux limit of 0.1 Jy, the calculations of Dabrowski et al. (1995) (their Figure 4) suggest that orientation bias

can be ignored. Nevertheless, in what follows I do not discount the possibility that this might not be the case.

The question of whether there is a correlation of the sort discussed above is easily settled; Figure 1 is a plot of projected linear extent  $d$  (as indicated by the measured angular size) against correlated rest-frame luminosity  $L$  (calculated assuming isotropic emission and a spectral index  $\alpha = 0.1$ , where  $L \propto \nu^\alpha$ ), for a selection of redshift bins, each containing 16 sources from the Gurvits (1994) sample. A cosmology is needed for this plot, and I have pre-empted the results to be presented here by using  $\Omega_m = 0.24$  and  $\Omega_\Lambda = 0.76$ ; however, the significant qualitative aspects of the arguments I shall present are not sensitive to this choice. The dashed line is a curve according to the Dabrowski et al. (1995) beaming model, for typical source parameters: actual luminosity  $10^{24}$  Watts/Hz, actual separation 65 parsecs and Lorentz factor 10. There is clear evidence that at any particular epoch individual luminosities are a function of size, and that for sources with  $z \gtrsim 0.2$  this relationship is an inverse correlation; empirically for  $z \gtrsim 0.5$  the relationship is well represented by

$$L = \mathcal{L}(z) \left( \frac{d}{\mathcal{D}} \right)^{-b} \quad 2 \lesssim d \lesssim 20 \text{ pc} \quad (1)$$

where the parameter  $\mathcal{D}$  and the exponent  $b$  do not depend upon  $z$ ; in round figures the exponent is  $b = 3$ . In a sample with flux limit  $F_1$ , equation (1) defines a cut-off linear size  $d_c$  by

$$d_c = \mathcal{D} \left( \frac{\mathcal{L}(z)(1+z)^{1+\alpha}}{4\pi d_L(z)^2 F_1} \right)^{1/b} \quad (2)$$

where  $d_L(z)$  is the luminosity distance at redshift  $z$ ; if  $d > d_c(z)$  the source will be too faint to be included in the sample. Figure 2 is a plot of linear extent against  $z$ , for all 337 sources in the Gurvits (1994) sample. If  $\mathcal{L}(z)$  is represented by a power law  $z^n$ , then  $d_c(z)$  is roughly constant if  $n = 2$ . If  $n > 2$  then we would expect Figure 2 to show evidence of cut-off effects at the low-redshift end of the diagram, which appears to be the case; the dash-dotted line in Figure 2 shows  $d_c(z)$  with  $\mathcal{D} = 1$  pc,  $\mathcal{L}(z) = 2 \times 10^{30} z^{4.5}$  Watts/Hz.

The premises upon which this work is loosely based are thus:

- (1) For  $z \gtrsim 0.2$  there is a stable population of sources, described by equation (1); the mean power at any particular epoch increases as  $z^n$ , with  $n \gtrsim 2$ , but otherwise the population is characterised by parameters which do not change.
- (2) For  $0.5 \lesssim d \lesssim 2$  luminosity evolution allows even the largest (and hence faintest) members of the population to remain within the flux-limited sample.
- (3) As  $z$  falls from 0.5 to 0.2 the mean luminosity begins to fall catastrophically, as the era of quasars and AGNs comes to a close, and we begin systematically to lose the larger members of the population due to selection effects.
- (4) Below  $z \sim 0.2$  the rapid decline in mean luminosity continues, and we see just the very smallest (and hence most powerful) members of a remnant population of intrinsically smaller objects.
- (5) For  $z \gtrsim 2$  there is some evidence that we are losing larger members of the population, possibly due to relativistic beaming effects.

In support of statement (5) Figure (2) includes the dashed curve showing a high-redshift cut-off according to the Dabrowski et al. (1995) model, with luminosity  $2 \times 10^{24}$  Watts/Hz, separation 130 pc and Lorentz factor 10. An alternatively explanation would be a down-turn in  $\mathcal{L}(z)$ .

It is probable that there is a unified picture here, just as there is for quasars and BL Lacertae objects (Blandford & Rees 1978; Padovani & Urry 1990). The underlying source population consists of compact symmetric objects (Wilkinson et al. 1994), comprising central bright cores traddled by two mini-lobes; their observed structures are not dominated by relativistic beaming. At a given redshift the sample will consist of such objects observed from the side, plus intrinsically weaker sources in which beaming is important, their relative frequencies being determined by the luminosity function. However, for the purposes of this paper it is important to know that there are selection effects which bias against larger objects, and to take measures to minimize their consequences. It should be stressed that these measures are empirical, and are not tied to a particular model of the objects in question.

### 3 COSMOLOGICAL PARAMETERS

As in Gurvits (1994) and Jackson & Dogson (1997), I shall consider only those sources with  $z > 0.5$ , amply justified by the above discussion. These are placed in redshift bins, and normally the means for each bin would be plotted in a  $\theta$ - $z$  diagram. However, if we believe that some of the larger members of the population have been lost, but none of the smaller ones, then the definition of mean angular size needs some attention. The sensible way forward is to define a lower envelope for the data. We might for example use the lowest point within each bin, but this is too noisy. I have defined the lower envelope as the boundary between the bottom third and the top two thirds of the points within each bin. Figure 3 shows 6 such composite points; each of these derives from a bin containing 42 objects, being the mean of points 11 to 17 within each bin, counting from the smallest object. Error bars are  $\pm$  one standard deviation as determined by the said points; they are shown as an indication of the efficacy of this definition of lower boundary, and are not used in the following statistical analysis. The sample comprises 252 objects in the range  $0.541 \leq z \leq 3.787$ . With respect to bin size, I find that 42 is the best compromise between noise reduction and a sensible number of points in Figure 3.

A simple three-parameter least-squares fit to the points in Figure 3 gives optimum values  $\Omega_m = 0.29$ ,  $\Omega_\Lambda = 0.37$  and mean projected separation  $d = 5.7$  parsecs. If the model is constrained to be flat, then a two-parameter least-squares fit gives optimum values  $\Omega_m = 0.24$ ,  $\Omega_\Lambda = 1 - \Omega_m = 0.76$  and  $d = 6.2$  parsecs, which model is shown as the continuous curve in Figure 3; the latter also shows the zero-acceleration model  $\Omega_m = 0$ ,  $\Omega_\Lambda = 0$ ,  $d = 6.2$  as the dashed curve. The difference  $\Delta\theta$  between the two curves is presented in Figure 4, which shows clearly the shift from acceleration to deceleration. Note however that the actual switch occurs before the crossing point, at  $z = (2\Omega_\Lambda/\Omega_m)^{1/3} = 0.85$  in this case, roughly where the dashed curve begins to swing back towards the continuous one. Figure 4 establishes definitively and accurately that there is no need to invoke anything other than a simple  $\Omega_m$ - $\Omega_\Lambda$  model to account for the data, out to a redshift  $z = 2.69$ . In this context the current record for SNe Ia is SN 1997ff at  $z \sim 1.7$  (Gilliand & Phillips 1998; Riess et al. 2001), with a somewhat uncertain apparent magnitude.

In order to derive confidence regions, I have defined a fixed standard deviation  $\sigma$  to be attached to each point in Figure 3:  $\sigma^2 = \text{residual sum-of-squares}/(n - p)$ , where  $n = 6$  is the number of points and  $p = 3$  is the number of fitted parameters, giving  $\sigma = 0.0099$  in this case. This value of  $\sigma$  is used to calculate  $\chi^2$  values at points in a suitable region of parameter space. Figure 5 shows confidence regions in the  $\Omega_m$ - $\Omega_\Lambda$  plane derived in this manner, marginalised over  $d$  according to the

scheme outlined in Press, Flannery, Teukolsky & Vetterling (1986). Without the extra constraint of flatness little can be said about  $\Omega_\Lambda$ , which degeneracy is due to the lack of data points with  $z < 0.5$  (Jackson & Dogson 1996). Nevertheless Figure 5 clearly constrains  $\Omega_m$  to be significantly less than unity. Figure 5 is essentially a refined and tighter version of the diagram presented in Jackson & Dodgson (1997); significant changes are that flat models are now well within the 68% confidence region, and the global optimum (indicated by the cross) is firmly in the positive quadrant, which changes can be attributed to the measures relating to selection effects. In the case of flat models, two-dimensional confidence regions can be presented without marginalisation. Figure 6 shows such regions in the  $\Omega_m$ - $d$  plane; marginalising over  $d$  gives 95% confidence limits  $\Omega_m = 0.24 + 0.09 / - 0.07$ . The central figure is quite robust, and is not for example sensitive to choice of binning; however, the various refinements introduced here have dramatically reduced the uncertainty: to the same level of detail figures in Jackson & Dodgson (1997) would have been  $\Omega_m = 0.24 + 0.32 / - 0.14$ .

As already noted with respect to Figure 4, simple  $\Omega_m$ - $\Omega_\Lambda$  models give an excellent fit to the data. Nevertheless, in conclusion I consider the limits placed upon the quintessence parameter  $w$ , defined by postulating an equation of state for the vacuum of the form  $\rho_{\text{vac}} = wp_{\text{vac}}$  relating the vacuum density  $\rho_{\text{vac}}$  to the vacuum pressure  $p_{\text{vac}}$ , with  $|w| \leq 1$  and  $w = -1$  corresponding to the conventional vacuum defined by a cosmological constant. For flat models we have a three-parameter system comprising  $\Omega_m$ ,  $w$  and  $d$ , the quintessence parameter  $\Omega_q$  being  $1 - \Omega_m$ ; we proceed by marginalising over  $d$  to give the two-parameter confidence regions shown in Figure 7. The system is highly degenerate, and with respect to material content cannot distinguish between for example a two component mix with  $\Omega_m = 0.24$ ,  $\Omega_q = 0.76$ ,  $w = -1$  at one extreme, and a single component compromise with  $\Omega_m = 0$ ,  $\Omega_q = 1$ ,  $w = -0.37$  at the other. Lacking any compelling evidence to the contrary, the sensible choice is to retain local Lorentz invariance and stick with  $w = -1$ .

## 4 CONCLUSIONS

The prescription adumbrated here has produced a set of data points which are remarkably consistent with  $\Omega_m$ - $\Omega_\Lambda$  FLRW cosmological models, but there is extensive degeneracy due to the restricted redshift range. This degeneracy is resolved by combining angular-size/redshift data with that CMBR information which indicates flatness, and the two data sets together give  $\Omega_m = 0.24 + 0.09 / - 0.07$ . This compares well with the figure  $\Omega_m = 0.27 \pm 0.04$  arising from WMAP measurements combined with a host of other astronomical data sets (Spergel 2003); in this context the points generated in this work might be added as an extra data set; for future reference these are given in Table 1.

Table 1. Data points for the angular-size/redshift relationship;  $\theta$  is in milliarcseconds.

$z$	$\theta$
0.623	1.277
0.845	1.089
1.138	1.034
1.450	1.023
1.912	1.008
2.686	1.024

This work builds upon the earlier work of Jackson & Dodgson (1997), and shows that the results obtained there were not spurious. Its purpose goes beyond that of showing compatibility with more recent work, and suggests that building a much larger angular-size/redshift data set for ultra-compact sources would be a promising enterprise, with view to an accurate and independent determination of the state of the local vacuum. However in this context I must end on a cautionary note; in general results from the 5Ghz sample due to Gurvits et al. (1999) are compatible with the ones discussed here, but with much greater uncertainty (Gurvits et al. 1999; Chen & Batra 2003); the prescription developed here does not significantly improve matters in this respect. Probable reasons for this difference in behaviour are easily discernable. Firstly, the 1999 compilation is not homogeneous, in that it comprises a number of sub-samples published by various authors; secondly, the definition of angular size is based upon contour maps and component separations (Kellermann 1993), rather than the totally objective measure based upon fringe visibility used here.

## REFERENCES

- Balbi, A. et al., 2000, *ApJ*, 545, L1  
Baldwin J.E., 1982, in Heeschen D.S., Wade C.M., eds,  
Proc. IAU Symp. 97, Reidel, Dordrecht, p. 21  
Blundell K.M., Rawlings S., 1999, *Nat*, 399, 330  
Barthel P.D., Miley G.K., 1988, *Nat*, 333, 319  
Blandford R., Rees M.J., 1978, in Wolfe A.N., ed,  
Proc. Pittsburgh Conf. BL Lac Objects, Pittsburgh: University of Pittsburgh Press, p. 328  
Bridle S.L., Eke, V.R., Lahav O., Lasenby A.N., Hobson M.P., Cole S., Frenk C.S., Henry J.P.,  
1999, *MNRAS*, 310, 565  
Chen G., Ratra B., 2003, *ApJ*, 582, 586  
Cunha J.V., Alcaniz J.S., Lima J.A., 2002, *Phys. Rev. D*, 66, 023520  
Dabrowski, Y., Lasenby, A., Saunders, R., 1995, *MNRAS*, 277, 753  
de Bernardis P. et al., 2000, *Nat*, 404, 955  
Dunlop, J.S., Peacock J.A., 1990, *MNRAS*, 247, 19  
Efstathiou G., Sutherland W.J., Maddox S.J., 1990, *Nat*, 348, 705  
Efstathiou G., Bridle S.L., Lasenby A.N., Hobson M.P., Ellis R.S., 1999, *MNRAS*, 303, 47  
Efstathiou et al., 2002, *MNRAS*, 330, 29  
Gilliland R.L., Phillips M.M., 1998, *IAU Circ.* 6810  
Gurvits L.I., 1994, *ApJ*, 425, 442  
Gurvits, L.I., Kellermann K.I., Frey S., 1999, *A&A*, 342, 378  
Hanany S. et al., 2000, *ApJ*, 545, L5  
Jackson J.C., 1973, *MNRAS*, 162, 11P  
Jackson J.C., Dodgson M., 1996, *MNRAS*, 278, 603  
Jackson J.C., Dodgson M., 1997, *MNRAS*, 285, 806  
Jain D., Dev A., Alcaniz J.S., 2003, *astro-ph/0302025*  
Kellermann K.I., 1972, *AJ*, 77, 531  
Kellermann K.I., 1993, *Nat*, 361, 134  
Lasenby A.N., Bridle S.L., Hobson, M.P., 2000, *Astrophys. Lett. & Communications*, 37, 327  
Legg, T.H., 1970, *Nat*, 226, 65  
Lima J.A.S., Alcaniz J.S., 2002, *ApJ*, 566, 15  
Masson C.R., 1980, *ApJ*, 242, 8  
Miley G.K., 1971, *MNRAS*, 152, 477  
Nilsson K., Valtonen M.J., Kotilainen J., Jaakkola, T., 1993, *ApJ*, 413, 453  
Ostriker, J.P., Steinhardt, P.J., 1995, *Nat*, 377, 600  
Padovani, P., Urry, C.M., 1990, *ApJ*, 356, 75  
Peebles P.J.E., 1984, *ApJ*, 284, 439  
Perlmutter S. et al., 1999, *ApJ*, 517, 565  
Press W.H., Flannery B.P., Teukolsky S.A., Vetterling W.T., 1986,  
Numerical Recipes, Cambridge University Press, Cambridge, pp. 532-536  
Preston R.A. et al., 1985, *AJ*, 90, 1599  
Richter G.M., 1973, *Astrophys. Lett.*, 13, 63  
Riess A.G. et al., 1998, *AJ*, 116, 1009  
Riess A.G. et al., 2001, *ApJ*, 560, 49  
Schmidt B.P. et al., 1998, *ApJ*, 507, 46  
Singal A.K., 1988, *MNRAS*, 233, 87  
Spergel D.N. et al., 2003, *astro-ph/0302209*  
Thompson A.R., Moran J.M., Swenson G.W., Jr, 1986,  
Interferometry and Synthesis in Radio Astronomy. Wiley, New York



Turner M.S., Steigman G., Krauss L.L., 1984, Phys. Rev. Lett., 52, 2090  
Wardle J.F.C., Miley G.K., 1974, A&A, 30, 305  
Wilkinson P.N., Polatidis A.G., Readhead A.C.S., Xu W., Pearson T.J., 1994, ApJ, 432, L87

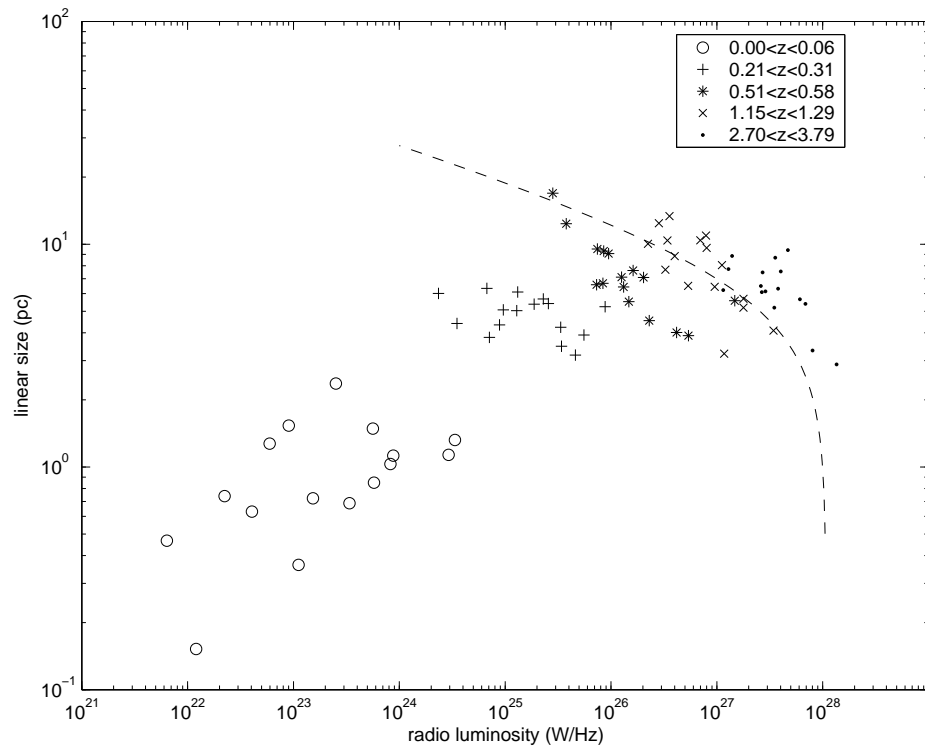


Figure 1: Linear size versus radio luminosity for sources in selected redshift bins, showing the inverse correlation between linear size and radio power at high redshifts. The dashed curve corresponds to a model in which relativistic beaming effects are dominant.

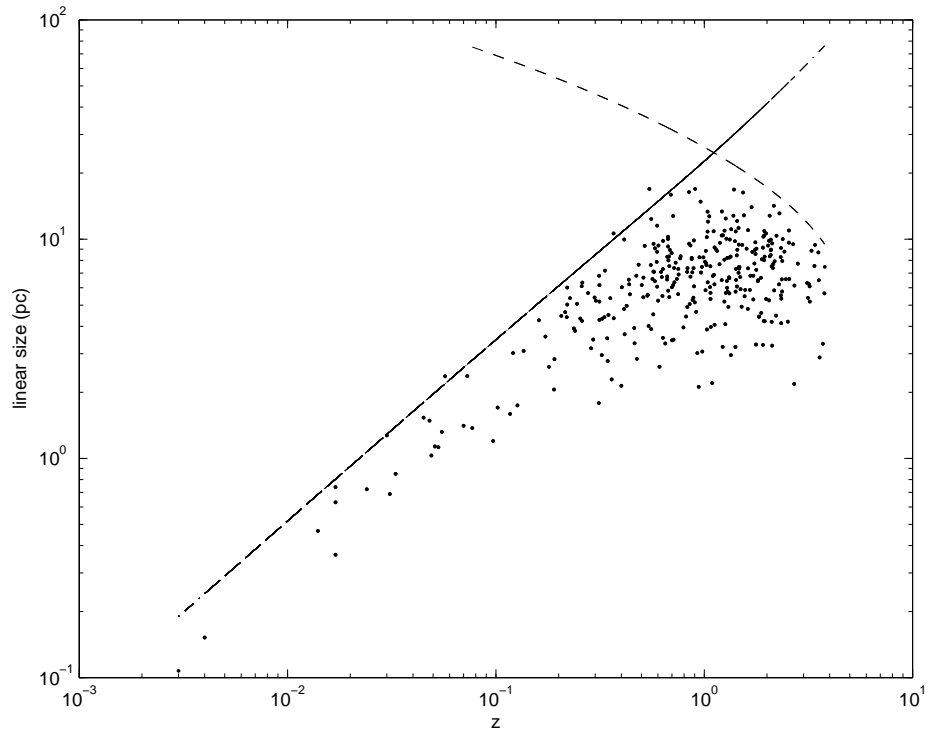


Figure 2: Linear size versus redshift for the 337 sources in the sample used here. The dashed curve shows a high-redshift selection cut-off according to a model in which relativistic beaming effects are dominant. The dash-dotted curve shows a low-redshift cut-off due to luminosity evolution.

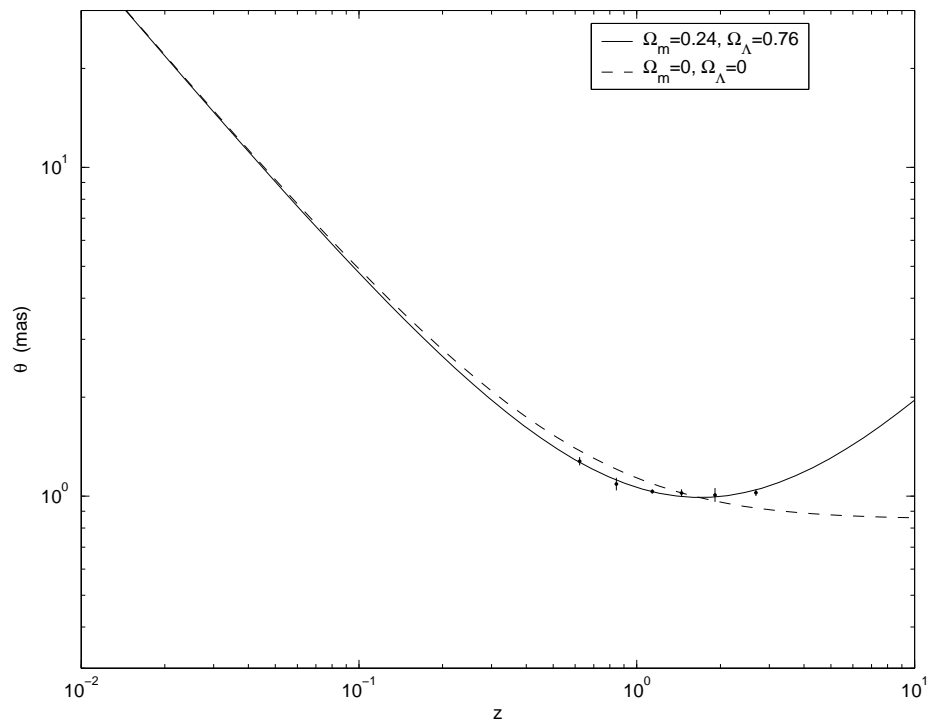


Figure 3: Angular size versus redshift for 252 sources with  $0.541 \leq z \leq 3.787$ , divided into 6 bins of 42 objects. The angular size corresponds roughly to the 14th object within each bin; this definition is used to eliminate the effects of bias against large objects. The continuous curve is the best flat one.

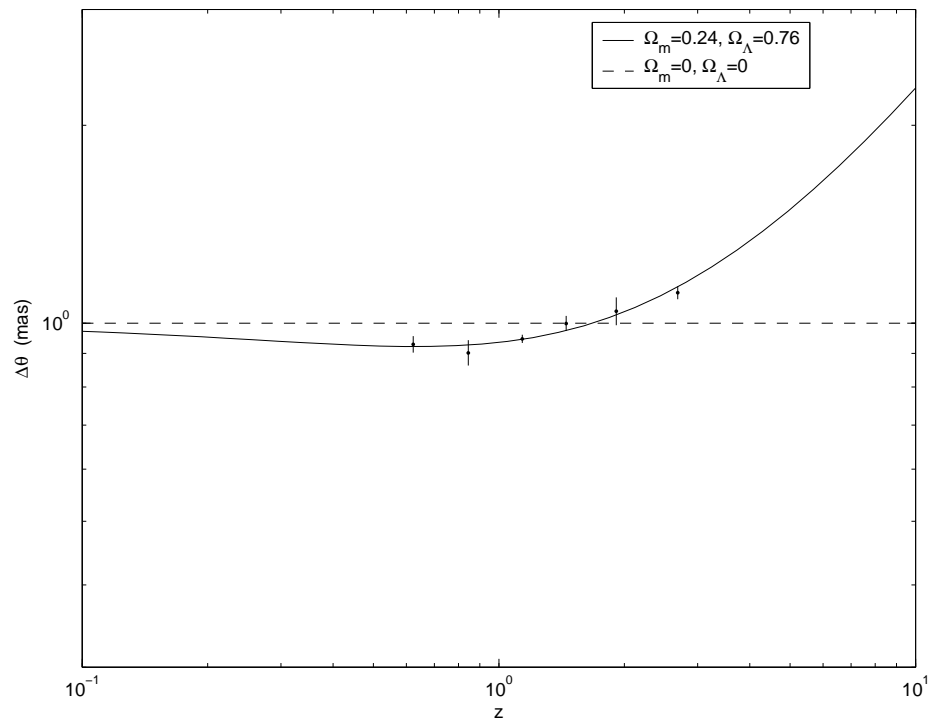


Figure 4: Differential form of Figure 3, showing the expected switch from acceleration to deceleration.

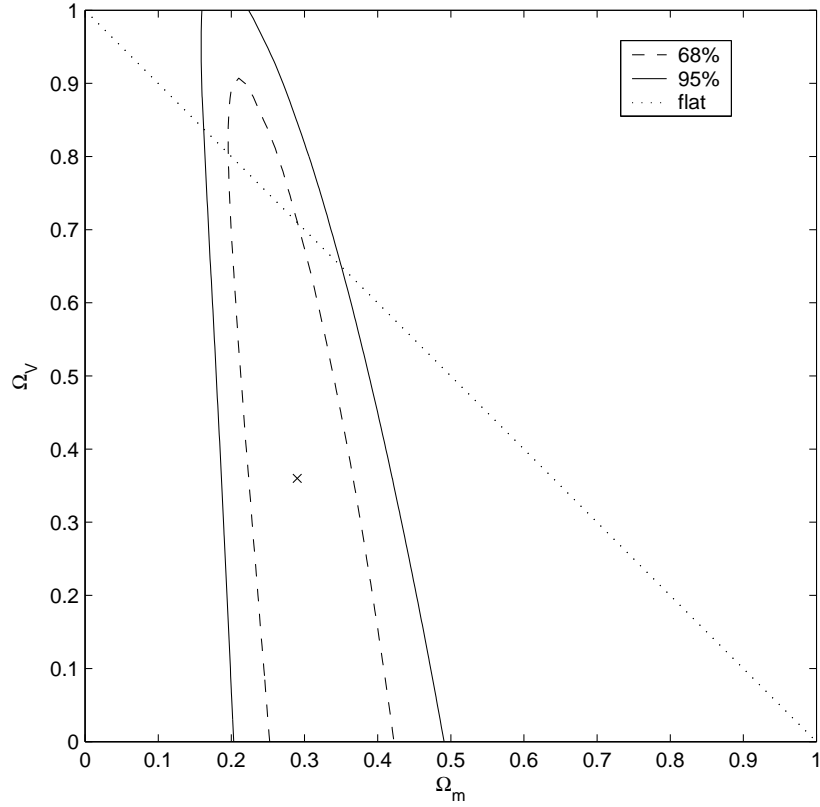


Figure 5: Confidence regions in the  $\Omega_m$ - $\Omega_\Lambda$  plane, marginalised over the linear dimension  $d$ ; the cross indicates the global minimum in  $\chi^2$ , at  $\Omega_m = 0.29$ ,  $\Omega_\Lambda = 0.37$ .

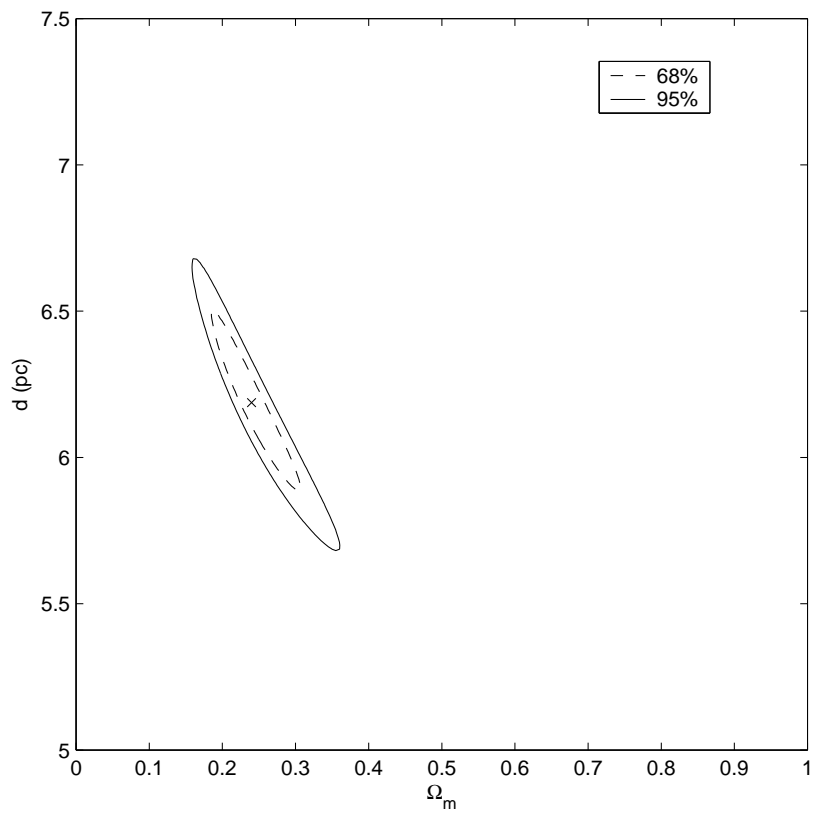


Figure 6: Confidence regions in the  $\Omega_m$ - $d$  plane for flat models; the cross indicates the minimum in  $\chi^2$ , at  $\Omega_m = 0.24$ ,  $d = 6.20$  pc. Marginalising over the linear dimension  $d$  gives  $\Omega_m = 0.24 + 0.09 / -0.07$ .

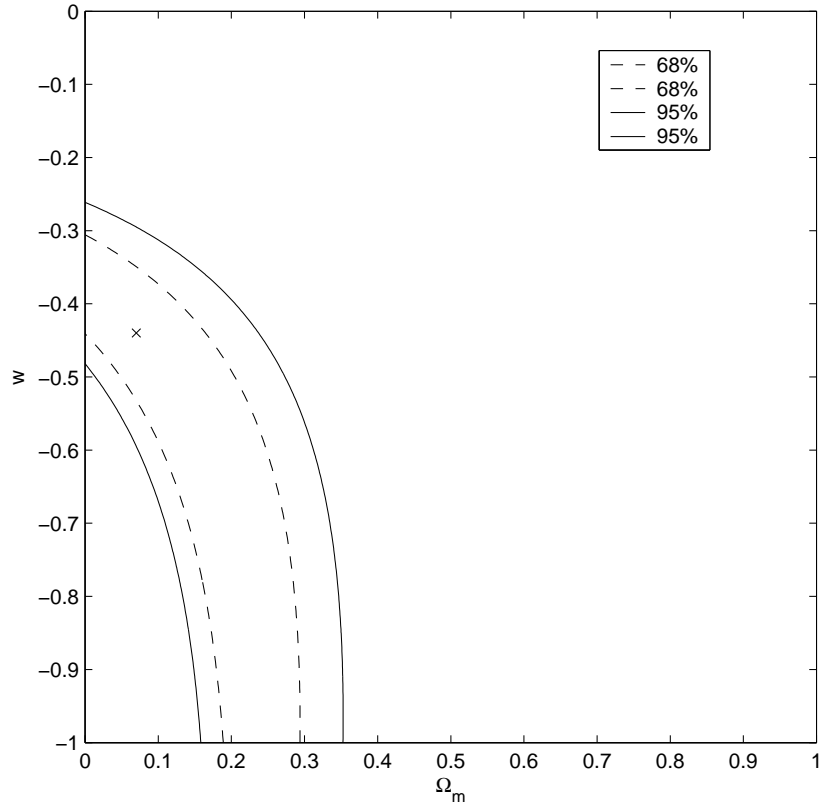


Figure 7: Confidence regions in the  $\Omega_m$ - $w$  plane for flat models, marginalised over the linear dimension  $d$ , where  $w$  is the quintessence parameter; the cross indicates the global minimum in  $\chi^2$ , at  $\Omega_m = 0.07$ ,  $w = -0.44$ .